TRIM27 is an autophagic substrate and putative regulator of LC3B

Juncal Garcia Garcia[1], Katrine Stange Overå[1], Erik Knutsen[2], Zambarlal Bhujabal[1], Gry Evjen[1], Trond Lamark[1], Terje Johansen[1], Eva Sjøttem[1]*

[1]*Molecular Cancer Research Group, Department of Medical Biology, University of Tromsø – The Arctic University of Norway, 9037 Tromsø, Norway*

[2]*RNA and Molecular Pathology Research Group, Department of Medical Biology, University of Tromsø –The Arctic University of Norway, 9037 Tromsø, Norway*

*Corresponding author. Tel: +47 776 46425; E-mail: eva.sjottem@uit.no

Running title: TRIM27 in autophagy and cancer

Keywords: TRIM27, autophagy, breast cancer, LC3B

ABSTRACT

Cells use autophagy, an evolutionary conserved catabolic process, to maintain proper homeostasis. Defects in autophagy have been associated with cancer, where it modulates cell resistance or sensitivity to therapy, in addition to affecting the migration and invasion capabilities of tumor cells. The tripartite motif-containing 27 (TRIM27) protein is highly expressed in various cancers including breast cancer, shown to be involved in a multitude of processes such as cell proliferation, transcriptional repression, apoptosis, STAT3 activation, inhibition of NF-kB activation, and innate immune response. Here we identify TRIM27 as an autophagic substrate, depending on ATG7 and the sequestosome-like receptors for its lysosomal degradation. We mapped a LIR motif within its coiled-coil regions, with highest specificity towards LC3C. Knock out of TRIM27 in HEK293 cells did not affect the starvation induced autophagy response, but affected p62 and LC3B protein levels under nucleotide mediated stress activating the innate immune response. Reintroduction of TRIM27 expression in TRIM27 KO cells inhibited cell proliferation but facilitated cell migration, suggesting that the oncogenic role of TRIM27 may be associated with epithelial-mesenchymal transition. mRNA expression profiling confirmed that TRIM27 is significantly upregulated in breast cancer tissue compared to normal tissue. Importantly, both TRIM27 and LC3B were aberrantly expressed in various breast cancer cell lines, and their expression levels seemed to be inversely correlated. Thus, these breast cancer cell lines represent potent model systems for identifying the roles of TRIM27 and autophagy in breast cancer.

INTRODUCTION

Synthesis and clearance of functional proteins regulate their availability within the cell, adapting the protein pool to the cellular needs. Thus, protein degradation is a crucial element in the maintenance of cellular homeostasis. Such an important process is tightly regulated in a spatially and timely manner through two main systems: the ubiquitin-proteasome system (UPS) and the lysosomal-mediated proteolysis (hereafter autophagy) (Dikic, 2017).

The main tag for degradation is a globular protein is a 76 amino acid component called ubiquitin. Targeted proteins are conjugated to ubiquitin by the mediation of three sequential reactions. The first reaction is the activation of ubiquitin by E1 enzymes. The second reaction consists in the conjugation of ubiquitin to E2 enzymes for its delivery to the next step. The third and last reaction is mediated by E3 ligases that make possible the binding of the activated ubiquitin with the target molecule. While E1 and E2 are highly conserved and do not present much specificity, E3 ligases are in charge of recognizing the substrate, which makes them the main regulator of the pattern of ubiquitination (Kleiger and Mayor, 2014). Ubiquitin can generate degradation signals by both the proteasome and the autophagic machinery. Thus, ubiquitin is a common denominator for both UPS and autophagy that work coordinately to create an efficient proteolytic network (Ji and Kwon, 2017). In the beginning, ubiquitin was identified as a simple tag for protein degradation. However, in the last decades, evidences have shown the important role of ubiquitination as a posttranslational modification in many cellular processes such as DNA repair response, cell cycle regulation, autophagy, cellular differentiation and cell-mediated immunity (Swatek and Komander, 2016, Kwon and Ciechanover, 2017, Yu and Matouschek, 2017).

Tripartite motif family proteins (TRIMs) are a wide family of proteins involved in the control of several cellular processes such as intracellular signaling, innate immunity, transcription, autophagy and carcinogenesis. To date, there are more than 80 distinct protein members in the TRIM family (Hatakeyama, 2017). The vast majority of those TRIMs present E3 ligase activity since they contain a RING finger-domain. Those TRIMs defined as E3 ligases are characterized by the presence of tripartite motif RBCC domain. The RBCC domain contains in the N-terminal one RING-finger domain, one or two B-boxes (B1/B2) and a coiled-coil (CC) domain. In addition, most TRIMs also present domains at the C-terminus, which gives them specificity for their target proteins (Esposito et al., 2017). TRIM proteins play several roles in autophagy, both as regulators and effectors. Some TRIMs, such as TRIM5α, 6, 16, 17, 20, 22, 49 and 55, act as a platform through the assembling of ULK1 and Beclin 1. This regulatory

complex has been name TRIMosome, which regulates selective autophagy (Mandell et al., 2014a). Other TRIMs, such as TRIM5α can also act as autophagy receptors of specific targets (Mandell et al., 2014b). Moreover, some TRIMs regulate autophagy through their interaction with p62 (Hatakeyama, 2017). This interaction often take place under certain cellular conditions, such as TRIM13 during ER stress (Tomar et al., 2012). This shows the high specificity of this family of E3 ligases. No TRIM homologs have been identified in yeast, which is well-studied autophagy model organism. Thus, TRIM proteins might add complexity to the mammalian autophagy system, being able to regulate more specific degradation processes.

TRIM27 is a E3 ligase also known as Ret finger protein (RFP protein), which was firstly described as a fusion protein with the tyrosine kinase domain of the c-RET proto-oncogene originated by DNA rearrangement (Cao et al., 1996). This 58 kDa protein can be found both in the cytoplasm and the nucleus of the cells, depending on the cell type (Tezel et al., 1999). TRIM27 is involved in the regulation of several cellular processes such as immunity, apoptosis, cell growth, proliferation and endosomal recycling (Chen et al., 2016, Zoumpoulidou et al., 2012, Liu et al., 2014, Zhuang et al., 2016). TRIM27 have been reported to have several roles in host defense against pathogens. TRIM27 acts as a host restriction factor during mycobacterial infection, enhancing immune-inflammatory response and cell apoptosis (Wang et al., 2016). In addition, TRIM27 has been identified as a degradation target of Herpes Simple Virus 1 ICP0, (Conwell et al., 2015) and together with USP7 negatively modulates antiviral type I INF signaling (Cai et al., 2018). Moreover, TRIM27 also plays a role in endosomal recycling when it is in complex with USP7 and MAGE-L2. This complex regulates the activity of the WASH/retromer-mediated endosomal recycling through its ubiquitination status (Hao et al., 2015). Furthermore, TRIM27 has been identified as an oncogene, highly expressed in various cancer types such as breast cancer. TRIM27 promotes proliferation mainly through its nuclear function, participating in transcriptional regulation complexes (Horio et al., 2012, Iwakoshi et al., 2012, Tsukamoto et al., 2009, Tezel et al., 2009, Chen et al., 2016, Zhang et al., 2018a, Zhang et al., 2018b) and also proposed to be involved in cell migration (Zhang et al., 2018b). However, whether TRIM27 plays a role in autophagy and cancer still need to be fully elucidated.

Here we show that TRIM27 is a cargo for the sequestosome-like receptors p62 and NDP52, directing it for lysosomal degradation. TRIM27 is localized in certain autophagic stuctures in the cytoplasm, and a LIR motif with specificity towards LC3C was identified in its coiled-coil region. TRIM27 did not seem to act as an autophagy receptor itself, nor did it affect

the autophagy process in HEK293 cells under normal and starved conditions. However, LC3B protein levels were stabilized in HEK293 FlpIn TRIM27 KO cells, and induction of autophagy seemed to be affected in these cells upon activation of the innate immune response. Furthermore, TRIM27 KO lead to enhanced cell proliferation, but strongly inhibited cell migration of the HEK293 FlpIn cells. In line with previous studies, our bioinformatics analysis show that TRIM27 expression is upregulated in breast cancer tissues. Interestingly, the expression of TRIM27 varies substantially in cells representing different breast cancer subtypes, and its expression level seemed to be inversely correlated with the expression of LC3B.

MATERIALS AND METHODS

Antibodies and reagents.

The following primary antibodies were used: rabbit polyclonal antibody for TRIM27 (Proteintech, #122205-1-AP)(1:1000); rabbit polyclonal anti-GFP (Abcam, ab290)(1:5000); rabbit polyclonal anti-LC3B (Sigma, L7543)(1:1000 for WB, 1:500 for IF); rabbit polyclonal antibody for phospho-4E-BP1 (Cell Signalling, #9451)(1:1000); mouse monoclonal anti-p62 lck ligand (BD Biosciences, 610833)(1:2000) and guinea pig polyclonal anti-p62 (Progen, GP62-C)(1:2000); mouse monoclonal anti-PCNA (DAKO, M0879)(1:1000) and rabbit polyclonal antibody anti-Beclin1 (Proteintech, #11306-1-AP)(1:1000). The following secondary antibodies were used: Horseradish-peroxidase (HRP)-conjugated goat anti-rabbit IgG (BD Biosciences, 554021)(1:2000); HRP-conjugated goat anti-mouse Ig (BD Biosciences, 554002)(1:2000); and HRP-conjugated anti-Biotin antibody (Cell Signalling, #7075)(1:2000). The following fluorescent secondary antibodies were used: Alexa Fluor® 488-conjugated goat anti-mouse IgG (Life Technologies, A-11029)(1:1000); Alexa Fluor® 555-conjugated goat anti-rabbit IgG (Life Technologies, A-11008)(1:5000); Alexa Fluor® 555-conjugated goat anti-mouse IgG (Life Technologies, A-21424)(1:1000); Alexa Fluor® 647-conjugated goat anti-guinea pig IgG (Life Technologies, A-21450)(1:1000). The reagents used were Bafilomycin A1 (Sigma, B1793); MG132 (Sigma, C2759); Tetracycline (Sigma, #87128); Hanks Balanced salt solution (Sigma, H8264).

Construction of Plasmids

All plasmids used in this study are listed in Table 1. Plasmids were made by use of the Gateway recombination system (ThermoFisher). Gateway LR reactions were performed as described in

the instruction manual. Point mutations were carried out using the Site-directed-mutagenesis kit from STRATAGENE. Primers for establishment of LIR mutated TRIM27$^{W184A/F186A/L189A}$ 5'-GAAGATTGTTGCGGAGGCTGAGCAGGCGTATCACTCCTTA-3' and Catalytic dead TRIM27$^{C16S/C19S}$ 5'-CAG GAG ACC ACC TCC CCC GTG TCC CTG CAG TAC TTC-3' were ordered from ThermoFisher. All plasmids were verified by restriction enzyme digestion and DNA sequencing (BigDye, Applied Biosystems, 4337455).

Table 1: Plasmids used in this study

pDONR221 TRIM27	Harvard HsCD00042999
pDest mCherry-EYFP TRIM27	(Overå et al., 2019)
pDest EGFP-C1	(Lamark et al., 2003)
pDest EGFP-TRIM27	This study
pDest Myc-TRIM27	This study
pDest Myc-TRIM27 LIRm	This study
pDest Myc	(Lamark et al., 2003)
pDest15 LC3A	(Pankiv et al., 2007)
pDest15 LC3B	(Pankiv et al., 2007)
pDest LC3C	(Alemu et al., 2012)
pDest GABARAP	(Pankiv et al., 2007)
pDest GABARAP L1	(Pankiv et al., 2007)
pDest GABARAP L2	(Pankiv et al., 2007)
pSPCas9(BB)-2A-GFP (PX458)	(Ran et al., 2013) Addgene#48138
pDONR TRIM27 CD	This study
pDest EGFP FlpIn FRT/TO	(Alemu et al., 2012)
pDEST EGFP FlpIn TRIM27	This study
pDEST EGFP FlpIn TRIM27 CD	This study

Cell culture and transfections

HeLa (ATCC, CCL2), Hek293 (ATCC, CRL-1573) and Hek293 T-Rex (ThermoFisher, R714-07) cells were cultured in Dulbecco's modified eagle's medium (DMEM) (Sigma, D6046) with 10% fetal bovine serum and 1% streptomycin-penicillin (Sigma, P4333). Hek FlpIn T-Rex cells with integrated EGFP-TRIM27, EGFP-TRIM27 CD were grown in the same medium with additional selection marker antibiotics, 200µg/ml Hygromycin B (Invitrogen, #10687010) and 7,5 µg/ml Blasticidin (Gibco, A1113903). The breast cancer cell lines HS578, MDA-MD-231, and MCF7 were cultured in DMEM medium. The breast cancer cell lines BT549, T47D, MDA-MD-468, BT474, HCC1569 and SKBR3 were cultured in RPMI-1640 medium. Sub-confluent

cells were transfected using TransIT-LT1 (Mirus, MIR2300) or Metafectene Pro (Biontex, T040) following the manufacturer's instructions. All cell lines were routinely tested for mycoplasma contamination.

Recombinant protein production and GST pulldown analysis

GST or GST-tagged proteins were expressed in *Escherichia coli* strain SoluBL21 (Genlantis, #C700200). Protein expression was induced by treating overnight bacterial culture with 50µg/ml Isopropyl β-D-1-thiogalactopyranoside (IPTG). GST or GST fusion proteins were purified and immobilized on Glutathione-Sepharose 4 Fast Flow beads (GE Healtcare, 17-5132-01). Myc-tagged proteins were *in vitro* translated using the TNT T7 reticulocyte Lysate system (Promega, #14610) in the presence of ^{35}S-methionine. *In vitro* translated protein or total cell lysate was pre-incubated with 10µl glutathione sepharose beads and 100µl of NETN buffer (50mM Tris pH 8.0; 150mM NaCl; 1 mM EDTA; 0.5% Nonidet P-40) with cOmplete Mini EDTA-free protease inhibitor mixture tablets (Roche Applied Science, 11836170001) for 1hr at 4°C to reduce unspecific binding. Pre-incubated lysate was then incubated with the immobilized GST fusion protein for 2hrs at 4°C. Beads were washed five times with NETN buffer, boiled with 2xSDS gel loading buffer (125mM Tris pH 7.5; 4% SDS; 0.04% bromphenol blue; 8% sucrose; 100mM dithiolthreitol) and subjected to SDS-PAGE. Gels were stained with Coomassie Brilliant Blue R-250 Dye (Thermofisher scientific, #20278) to visualize GST fusion proteins and then vacuum-dried. Signals from ^{35}S-labelled proteins were detected by a Fujifilm bioimaging analyzer BAS-5000 (Fujifilm).

Peptide Array

TRIM27 peptide arrays were synthesized on cellulose membranes using MultiPrep peptide synthesizer (INTAVIS Bioanalytical Instruments AG, Germany). Membranes were blocked with 5% non-fat dry milk in TBST and peptide interactions were tested with GST and GST-GABARAP by overlaying the membrane with 1 µg/ml of recombinant proteins and incubation for 2 h at room temperature. Bound proteins were visualized with HRP-conjugated anti-GST antibody.

Western Blotting

Cells were seeded in 6 well dishes and treated as indicated. Cells were lysed in 1xSDS buffer (50mM Tris pH 7.4; 2% SDS; 10% Glycerol) supplemented with 200mM dithiothreitol (DTT,

Sigma, #D0632) and heated at 100°C for 10 minutes. Protein concentration was measured using the Pierce BCA Protein Assay Kit (Thermofisher Scientific, #23227). Equal amounts of protein were resolved by SDS-PAGE and transferred to nitrocellulose membrane (Sigma, GE10600003). The membrane was stained with Ponceau S (Sigma, P3504), blocked with 5% non-fat dry milk in 1% TBS-T (0.2M Tris pH 8; 1.5M NaCl and 0.05% Tween20 (Sigma, P9416)) and then incubated with indicated primary antibodies for 24h. The membrane was washed three times for 10 minutes each with TBS-T followed by incubation with secondary antibody for 1h. The membrane was washed three times for 10 minutes and analyzed by enhanced chemiluminescence using the ImageQuant LAS 4000 (GE Lifescience).

Immunostaining and Fluorescence confocal microscopy

Subconfluent cells grown in 24-well plates on coverslips (VWR, #631-0150) coated with Fibronectin (Sigma, F1141) and treated as indicated. They were fixed in 4% paraformaldehyde for 20 min.The cells were then permeabilized with methanol at RT for 5min, blocked in 5% goat serum/PBS or 5%BSA/PBS and incubated at room temperature with a specific primary antibody followed by Alexa Fluor 488, 555 or 647 conjugated secondary antibody and DAPI. Confocal images were obtained using a 63x/NA1.4 oil immersion objective on an LSM780 (Zeiss). The line-profile tool in the ZEN software was exploited to plot co-localization of EGFP-TRIM27 and immunostained p62 and LC3B. Quantification of cells containing red only dots in the double tagged screen was done manually in three independent experiments.

Generation of TRIM27 knock out in HEK293 FlpIn cell lines

To generate knock out cells for TRIM27, the CRISPR/Cas9 system was exploited as described by (Ran et al., 2013). The Guide RNA sequence 5′-CTTTACCAGTTGGGTCACGT-3′ was ligated into the vector pSpCas9(BB)-2A-GFP (PX458) (Addgene, #48138) using BbsI restriction sites. Subconfluent Hek293 FlpIn T-Rex cells were transfected with the targeting plasmid using Metafectene Pro (Biontex, T020). EGFP-positive cells were sorted by FACS and plated into 96-wells plates three days post transfection. Single colonies were expanded up to 12-well plates and KO validated by immunoblotting. Confirmed KO clones were further screened by genomic sequencing. The targeted genomic regions were amplified by PCR using the primers 5'-CCGGAGAGAGCGCCGGAGAGTTG-3′ and 5′-CAAGGTGAGGGCGCGGATCCGGGAG-3′ and the resulting PCR products ligated into the pGEM-T-EASy vector (Promega, A3600). Sequencing were conducted for at least 3 clones for each PCR product.

Generation of tetracycline inducible HEK293 FlpIn cell lines

Stable cell lines were generated using the FlpIn T-Rex system (Thermofisher, R71407). TRIM27 cDNA was transferred to the inducible FlpIn expression vector pDest-EGFP-Flp-In (Alemu et al., 2012) by GATEWAY cloning. FlpIn T-Rex cells were then cotransfected with the TRIM27 FlpIn expression vector and the FlpIn recombinase vector pOG44 in the ratio of 1:3. Cells were selected by treatment with 200µg/ml Hygromycin B (Invitrogen, #10687010) and 7,5 µg ml^{-1} Blasticidin (Gibco, A1113903), and protein expression verified by induction with Tetracycline (Sigma, #87128).

Cell proliferation assay

The cell lines HEK293 T-Rex FlpIn, HEK293 T-Rex FlpIn TRIM27 KO, HEK293 T-Rex FlpIn TRIM27 KO + TRIM27 WT and HEK293 T-Rex FlpIn TRIM27 KO + GFP were harvested with trypsin and seeded into 12-well plates at a density of 100.000 cells per well. Afterwards, cells were incubated in IncuCyte (Essen BioScience, Ann Arbor, MI, USA) at 10x magnification and images were taken in the phase and green channels every 24h. Images were analyzed by Incucyte S3 Live-cell analysis system. The assays were performed in triplicate.

Migration assay

The cell lines HEK293 T-Rex FlpIn, HEK293 T-Rex FlpIn TRIM27 KO, HEK293 T-Rex FlpIn TRIM27 KO + TRIM27 WT and HEK293 T-Rex FlpIn TRIM27 KO + GFP were harvested with trypsin and seeded into 96-well Image-Lock Microplate (Essen BioScience, Ann Arbor, MI, USA) at a density of 80.000 cells per well. Twenty-four hours after seeding, a scratch wound was made by using the Incucyte 96-well WoundMaker tool (Essen BioScience, Ann Arbor, MI, USA) according to the manufacturer's instructions. Cells were incubated at 37 °C with CO2 in the Incucyte (Essen BioScience, Ann Arbor, MI, USA) at 10x magnification and pictures were taken in the phase and green channels every 15h (for figure presentation, quantification ever 24 hours is shown). Images were analyzed by Incucyte S3 Live-cell analysis system. The assay was repeated independently two times.

Bioinformatics

For the analysis of TRIM27 expression in normal versus tumor, two publically available breast cancer datasets, PRJNA399721 and PRJNA172761, were downloaded from the Sequence Read Archive (SRA). Since the data is publically available, REK approval is not necessary.

PRJNA399721 consist of 22 primary invasive breast cancer carcinoma expressing estrogen receptors and their paired adjacent mammary healthy tissues. Libraries were prepared using the TruSeq® Stranded Total RNA kit and Ribo-Zero rRNA Removal kit (Illumina) and sequencing was performed by strand-specific RNA sequencing on a Illumina HiSeq. PRJNA172761 consist of 53 primary breast cancers and 6 normal breast samples from mammoplasty patients. Single-end Illumina-based RNA-sequencing was performed, using both 29 bp reads (on 29 tumor samples) and 100 bp reads (on 24 tumor samples and 6 normals).

The CLC Genomic workbench (v8.5.1) was used for analyzing the RNA-Seq data. Raw reads were trimmed for quality (Quality limit = 0.05) and adaptor (Illumina TruSeq LT and HT adaptor or Illumina 1.5 Small RNA). Trimmed reads were mapped to GRCh38 with Ensembl annotation v84, using either strand specific mapping (PRJNA399721) or non-strand specific mapping (PRJNA172761), (Mismatch cost = 2, Insertion cost = 3, Deletion cost = 3, Length fraction = 0.9, Similarity fraction = 0.8). Only uniquely mapped reads were included in gene quantification. Reads per million (RPM) normalization was utilized, and gene counts were log2 transformed. Graphpad prism was used for making illustrations and statistical analysis. A paired t-test was used for the comparison of paired tumor versus normal samples, while a non-paired t-test was used for the calculation of normal versus tumor samples.

Statistics

All experiments were repeated at least three times, unless otherwise specified. Error bars represent the s.d. or s.e.m. as indicated in Figure legends. Replicates were not pooled for statistical analyses.

RESULTS AND DISCUSSION

In a qualitative screen in HeLa cells using the double tag mCherry-EYFP fused to 22 various members of the TRIM family of ubiquitin E3 ligases, we identified TRIM27 as a potential target for autophagic degradation (Fig. 1A) (Overå et al., 2019). Both under normal and starved conditions, RedOnly puncta could be observed in the mCherry-EYFP-TRIM27 expressing cells (Fig. 1A), with a slightly increased induction of RedOnly puncta upon starvation (Fig. 1D). To pinpoint the autophagy pathway implicated in TRIM27 degradation, the mCherry-EYFP-TRIM27 double tag assay was performed in ATG7 KO cell lines. We were not able to observe any RedOnly dots in the transfected ATG7 KO cell lines (Fig. 1B, upper panel). Previously, we have shown that autophagic degradation of TRIM32 is mediated by selective autophagy

involving the Sequestosome-Like-Receptors (SLRs). To investigate if also TRIM27 is degraded by selective autophagy mediated by the SLRs, the mCherry-EYFP-TRIM27 double tag assay was applied on a cell line knocked out for the five SLRs p62/SQSTM1, NBR1, NDP52, Optineurin and Tax1BP1 (pentaKO). No RedOnly dots of mCherry-EYFP-TRIM27 could be observed neither under normal nor starved conditions (Fig. 1B, middle panel). Together, these results indicate that autophagic degradation of TRIM27 is mediated by selective autophagy. Next, the mCherry-EYFP-TRIM27 double tag assay was applied on a HEK293 FlpIn cell line knocked out for p62/SQSTM1 (Overå et al., 2019). Some RedOnly dots could be observed in this cell line both under normal and starved conditions (Fig. 1B, lower panels), suggesting that autophagic degradation of TRIM27 is not dependent on p62. To measure whether p62 is sufficient to direct TRIM27 to autophagic degradation, we applied the mCherry-EYFP-TRIM27 double tag assay on the HeLa penta KO cell line reconstituted with EGFP-p62 (Fig. 1C) (Overå et al., 2019). Reintroduction of EGFP-p62 facilitated formation of mCherry-EYFP-TRIM27 RedOnly dots, but not to the same extent as the wild type cells (Fig. 1D). Similar results were obtained by reintroduction of EGFP-NDP52 (Fig. 1C,D). Thus, both SLRs were able to direct autophagic degradation of mCherry-EYFP-TRIM27. To sum up, here we suggest that TRIM27 is a cargo for selective autophagy, and its dependence on the SLRs for autophagic degradation indicates that it does not act as an autophagy receptor itself.

In order to determine if endogenous TRIM27 is degraded by autophagy, we analysed the TRIM27 protein levels in the ATG7KO and pentaKO cell lines. Importantly, for both cell lines endogenous TRIM27 protein levels were increased both in normal and starved conditions compared to normal HeLa cells (Fig. 2A), suggesting inhibited turnover of TRIM27 when selective autophagy is impaired. This was further supported by analysis of endogenous TRIM27 protein levels in a cell line knocked out for all six mammalian ATG8 proteins (kindly provided by Birendra Kumar Shrestha, unpublished)(Fig. 2A, lower panels). Together, these results show that selective autophagy is important for the regulation of TRIM27 protein levels.

TRIM proteins interacting with core components of the autophagy machinery are identified (Kimura et al., 2015, Kimura et al., 2016, Mandell et al., 2016, Mandell et al., 2014b) and recently we showed that TRIM32 binds weakly to p62 and the ATG8s *in vitro*, and colocalizes with p62 and LC3B in specific puncta in cell cytoplasm (Overå et al., 2019). TRIM27 is reported to be localized both in the cytoplasm and in the nucleus (proteinatlas.org), and hetero-oligomerization with TRIM19 (PML) recruites TRIM27 to promyelocytic leukaemia nuclear bodies (PMLs) in the nucleus (Cao et al., 1998). To investigate if TRIM27 may colocalize with autophagic structures in the cell, we established HEK293 FlpIn cells with

tetracycline inducible expression of EGFP-TRIM27. Co-staining of the tetracycline-induced HEK293 FlpIn EGFP-TRIM27 cell line with antibodies against p62 and LC3B, displayed co-localization of all three proteins in specific dots in the cytoplasm (Fig. 2B), suggesting recruitment of TRIM27 to autophagic structures. TRIM27 belongs to the same TRIM family subclass as TRIM5α, a retroviral restriction factor acting during the early post entry stages of the retroviral life cycle to block infection by a broad range of retroviruses, disrupting reverse transcription and integration (Forshey et al., 2005). In 2014 Trim5α was reported to act as a selective autophagy receptor, targeting a restricted virus to the autophagosome for degradation (Mandell et al., 2014b). They demonstrated that TRIM5α interacts directly with ATG8 proteins via a LIR motif. Later, the LC3 interacting region in TRIM5α was proposed to be located in a helical region within the coiled-coil region, including the residues D192, W196 and E203 (Keown et al., 2018). The similarity of TRIM5α and TRIM27 prompted us to apply a peptide array to identify putative ATG8 interacting regions in TRIM27. In this assay various 20 amino acid long peptides covering the complete region of TRIM27 were spotted on filter paper and probed against GST-GABARAP proteins expressed and purified from *E. coli*. The spot blot identified a putative LIR located within the W184-F186-L189 region of TRIM27 (Fig. 2C). To verify this putative LIR, we established the TRIM27$^{W184A/F186A/L189A}$ mutant (named LIRm) and compared its ability to bind the ATG8s with the binding ability of wild type TRIM27 in a GST-pulldown assay using GST-ATG8 proteins expressed and purified from *E. coli*, and TRIM27 proteins produced by *in vitro* translation. Figure 2C shows that wild type TRIM27 binds weakly to LC3C, GABARAP and GABARAPL1, and not at all to LC3B and GABARAPL2. Introduction of the LIRm mutations in TRIM27 resulted in strong reduction of the LC3C binding, and some reduction in the binding to GABARAP and GABARAPL1 (Fig. 2D). This suggests that TRIM27 contains a LIR with highest specificity against LC3C, located close to or within its coiled-coil region. The specificity for LC3C and partially GABARAP was further verified by GST-pulldown assay using cell extracts from the HEK293 FlpIn EGFP-TRIM27 cell line (Fig. 2E). Previously it is found that NDP52 interacts specifically with LC3C via a so-called CLIR motif, and this interaction was proposed to be crucial for innate immunity since cells lacking either protein was not able to protect their cytoplasm against Salmonella (von Muhlinen et al., 2012). Importantly, TRIM27 regulates innate immune responses by physical interaction with NOD2. TRIM27 mediates K48-linked ubiquitination and subsequent proteasomal degradation of NOD2 (Zurek et al., 2012). Together, these findings may suggest that TRIM27 represent a link between innate immunity and selective autophagy. As presented

in Fig. 1, the SLRs p62 and NDP52 are able to direct TRIM27 to autophagic degradation. To investigate if TRIM27 binds directly to these SLRs, we applied GST-pulldown assay of *in vitro* translated TRIM27 with GST-p62 and GST-NDP52. TRIM27 bound weakly to both proteins (Fig. 2E). To sum up, here we show that TRIM27 co-localize with p62 and LC3B in autophagic structures. It contains a LIR motif with highest specificity towards LC3C, and is dependent on at least p62 or NDP52 for autophagic degradation. Thus, TRIM27 seems to be a substrate for selective autophagy, but does not act as an autophagy receptor itself.

Next we set out to elucidate if TRIM27 impact on the autophagy process. For this purpose we established HEK293 FlpIn TRIM27 KO cell lines by the CRISPR/Cas9 technology (Ran et al., 2013). It is well recognized that p62 and LC3B colocalizes in certain cytoplasmic dots indicative of autophagosomes in HEK293 cells, and that the number of dots increases upon starvation due to induction of autophagy (Bjorkoy et al., 2005, Pankiv et al., 2007). Starvation induced autophagy is initiated by activation of ULK1, leading to phosphorylation of the ULK1complex members ATG13 and FIP200. Subsequently, the BECLIN1 complex including the VPS34 lipid kinase is activated and produces a pool of phosphatidylinositol 3-phosphate (PtdIns(3)P) at membrane sites where formation of the omgasome take place. Generation of PtdIns(3)P facilitates recruitment of WIPI2 (WD-repeat PtdIns(3)P effector protein) which can be observed as specific starvation induced WIPI2 dots by immunostaining (Karanasios et al., 2013, Koyama-Honda et al., 2013, Polson et al., 2010). WIPI2 recruits LC3B via the LC3 conjugation system to the forming omegasome (Dooley et al., 2014). Co-staining of p62, LC3B and WIPI2 in the TRIM27 KO cells under normal and starved conditions, indicated that initiation of the autophagy process were unaffected by TRIM27 ablation (Fig. 3A). As in the mother HEK293 FlpIn cell line, p62 and LC3B colocalized in certain cytoplasmic dots in the TRIM27 KO cells cultured in normal medium, and the number of such dots increased by changing the medium with HBSS for 2 hours. Moreover, the number of WIPI2 dots in the TRIM27 KO cells increased similarly as in the wild type cells upon starvation, and most of these dots co-localized with p62 and LC3B (Fig.3A). Thus, the starvation induced initiation of autophagy seems to be unaffected in the TRIM27 KO cells. Further analysis of LC3B lipidation in the TRIM27 KO cells by Western blotting, indicated that the amount of lipidated LC3B is similar in the TRIM27 KO cells as in the mother cell line (Fig.3B). Similarly, the protein levels of BECLIN1 and Tank Binding Kinase 1 (TBK1) were unaffected by TRIM27 KO (Fig. 3B). Previously, TRIM27 in shown to induce TBK1 degradation via K48-linked ubiquitination at Lys251 and Lys372 promoted by Siglec1 in interferon type I mediated antiviral innate immune response (Zheng et al., 2015). However, the unlipidated form of LC3B seemed to be stabilized

in the TRIM27 KO cells – and this stabilization was reproducible observed in various Western blots of TRIM27 KO cell extracts (i.e. Fig. 3D).

In view of the knowledge that TRIM27 is implicated in innate immune responses (Zurek et al., 2012; Zheng et al., 2015), and that autophagy plays important roles in innate immune responses to viral, bacterial, and fungal pathogens (reviewed in (Kuo et al., 2018)), we next questioned if TRIM27 could impact autophagy during activation of the innate immune response. Since the E3 ligase activity of TRIM27 is important for its regulation of the immune response, we established HEK293 FlpIn cell lines with tetracycline inducible expression of catalytic dead EGFP-TRIM27 (EGFP-TRIM27 CD). To activate the innate immunity, we transfected plasmid DNA (Myc) into the FlpIn EGFP-TRIM27 CD cell line, the FlpIn TRIM27 KO cell line and the wild type HEK293 FlpIn cell line. Interestingly, p62 protein levels is strongly accumulated in the cells expressing catalytic dead TRIM27, even though the mutated TRIM27 is expressed at much lower levels than endogenous TRIM27 (Fig. 3C). Since p62 degradation is unaffected by TRIM27 KO, but highly affected by expression of catalytic dead TRIM27, this may indicate that E3 ligase deficient TRIM27 induces formation of protein aggregates that recruits p62. Noteably, analyzing the LC3B protein levels in the same cell extracts, revealed that the amount of LC3B is strongly reduced in the cells expressing E3 ligase inactive TRIM27 (Fig. 3D). Together, these results indicate that the autophagic flux is strongly impaired by over-expression of catalytic dead TRIM27. Conversely, we observe that degradation of the LC3B I form is stabilized in the TRIM27 KO cells. Similarly as for p62, the starvation-induced turnover of LCB3 is inhibited in the TRIM27 KO cell lines upon transfection. Together, these results show that starvation-induced degradation of p62 and LC3B does not take place in HEK293 FlpIn TRIM27 KO cells when the cells are stressed by plasmid transfection. Next, we induced the innate immune response in the HEK293 FlpIn and TRIM27 KO cell lines by adding poly(IC) and poly(AT), mimicking infections by RNA or DNA viruses, respectively. Analysis of p62 protein levels in these cells, showed that addition of poly(AT) to the TRIM27 KO cells inhibited starvation-induced degradation of p62. This supports that TRIM27 may have a regulatory effect on autophagy induction under immunity stress conditions.

To further address if TRIM27 may impact the autophagy process, we established a HEK293 FlpIn TRIM27 KO cell line with tetracycline inducible expression of EGFP-TRIM27, and a HEK293 FlpIn TRIM27KO cell line with inducile expression of EGFP as control cell line (Fig. 4A). EGFP-TRIM27 in the reconstituted TRIM27 KO cell line localized to certain dots/aggregates in the cytoplasm, in addition to a few nuclear dots. This is in line with the

reported localisation of endogenous TRIM27 (proteinatlas.org). Next, we compared the proliferation and migration potential of the HEK293 FlpIn TRIM27 KO cells with the reconstituted TRIM27 KO cell lines (Fig. 4B). The HEK293 FlpIn TRIM27 KO cell line displays an enhanced proliferation rate compared to the HEK293 FlpIn TRIM27 KO cell line reconstituted with EGFP-TRIM27 (Fig. 4B, left graph). This suggests that TRIM27 expression inhibits cell proliferation. Conversely, the migration rate of the TRIM27 KO cells was reduced compared to the HEK293 FlpIn cells, while reintroduction of EGFP-TRIM27 restored the migration rate (Fig. 4B, right graph). Thus, in HEK293 FlpIn cells TRIM27 seems to inhibit cell proliferation while it facilitates cell migration. TRIM27 was originally identified as a gene involved in the oncogenic rearrangements with the RET proto-oncogene (Takahashi and Cooper, 1987). Later it is shown that TRIM27 is highly expressed in various cancers including breast, endometrial, ovarian, lung, colon and colorectal cancer, and colitis and colitis-associated carcinogenesis (Horio et al., 2012, Iwakoshi et al., 2012, Tsukamoto et al., 2009, Tezel et al., 2009, Ma et al., 2016, Zhang et al., 2018a, Zhang et al., 2018b). In these studies TRIM27 has been proposed as a oncogene promoting cell proliferation, and the mechanisms have been connected to its nuclear function participating in transcriptional regulation complexes. The proliferation and migration studies in the HEK293 FlpIn cells suggest that TRIM27 may be implicated in epithelial-mesencymal transition (EMT), which is in line with a recent study showning TRIM27 to activate EMT in colorectal cancer (Zhang et al., 2018b) and to promote anchorage-independent growth of various cell lines (Zhang et al., 2018a).

Our results so far suggest TRIM27 to be a autophagy substrate with a potential role in EMT. It is well recognized that there is a complex crosstalk between autophagy and EMT processes. At the early stages of metastatization, autophagy acts as oncosuppressive signal, tending to inhibit the EMT programme mainly by destabilizing EMT crucial players. Later on, metastatic cells require autophagy to survive to environmental and metabolic stressful conditions (reviewed in (Colella et al., 2019)). Upregulated TRIM27 expression has been associated with breast cancer and mechanistically this has been linked to its nuclear role implicated in Estrogen Receptor transcription complexes (Townson et al., 2006) and associated with HER2 status (Tezel et al., 2009). In order to investigate if TRIM27 expression is associated with autophagy activity in breast cancer, we first analysed the TRIM27 mRNA expression in tumor tissue and normal tissue from two different patient cohorts (Fig. 4C). In both cohorts, TRIM27 mRNA was significantly upregulated in the cancer tissues compared to normal tissue. Next, the amount of TRIM27 and LC3B proteins in various breast cancer cell lines representing various breast cancer subtypes were analysed by western blotting (Fig. 4D). The TRIM27

expression level varies substantially within the the various cell lines, with high expression in the luminal cell lines MCF7 and T47D, and in the basal-like cell ine MDA-MD-468. Moreover, in the MDA-MD-468 cells, the TRIM27 protein migrates slower suggesting that it may represent a TRIM27 fusion protein, or a TRIM27 protein highly modified by post-translational modifications. TRIM27-RET fusions are described in several cancers, however has not been detected in breast cancer (Hameed et al., 2009). In contrast, in the trippel-negative MDA-MD-231 and BT549 cell lines, no TRIM27 expression could be detected. Interestingly, LC3B was highly expressed in the triple-negative cell lines, while it was low in luminal and Her2 positive cell lines. Hence, the expression of TRIM27 and LC3B seems to be inversely correlated in the breast cancer cells, which is in line with our observations of stabilisation of LC3B in TRIM27 KO cells (see Fig. 3B,D). This suggests that TRIM27 may impact autophagy in breast cancer cells, and that breast cancer cell lines with various expression levels of TRIM27 represent promising model systems for further revealing the molecular mechanisms of TRIM27 in autophagy and cancer.

ACKNOWLEDGEMENT

We thank Richard Youle, National Institutes of Health, Bethesda, MD 20892, USA, for the generous gift of the pentaKO cell line, Yakubu P. Abudu, UiT – The Arctic University of Norway, for the gift of the EGFP-NDP52 and EGFP-p62 reconstituted pentaKO cell lines and the HeLa p62 KO cell line, and Birendra Kumar Shrestha, UiT – The Arctic University of Norway, for the gift of the ATG8 KO cell line. Thanks to the Advanced Microscopy Core Facility at UiT – The Arctic University of Norway, for the use of instrumentation. This work was supported by PhD grants to K.S.O and J.G.G from UiT – The Arctic University of Norway, and by the Research Council of Norway (TOPPFORSK program grant #249884 to T.J).

FIGURE LEGENDS

Figure 1: Autophagic degradation of TRIM27 is dependent on ATG7 and the Sequestosome-Like receptors. A) Confocal images of mCherry-EYFP-tagged TRIM27. HeLa cells were transfected with mCherry-EYFP-TRIM27 expression constructs one day before exposure to normal medium (FM) or starved medium (SM)(HBSS, 2 hours), fixation and imaged using a Zeiss780 confocal microscope and the Zen software. Scale bar (10 μm). **B)** HeLa cells that were genetically knocked out for ATG7 or the 5 autophagy receptors p62/SQSTM1, NBR1, NDP52, Optineurin or Tax1BP1 (pentaKO) or p62/SQSTM1 (a generous gift from Yakubu P. Abudu) were transfected with mCherry-EYFP-TRIM27. One day post transfection half of the cells were treated with HBSS for 2 hrs (SM), before all cells were fixated, stained with DAPI and imaged using a Zeiss780 confocal microscope. Scale bar (10 μm). **C)** Normal HeLa cells and cells that were genetically knocked out for the 5 autophagy receptors p62/SQSTM1, NBR1, NDP52, Optineurin or Tax1BP1 (pentaKO), pentaKO cells with reintroduced GFP-NDP52 or pentaKO cells with reintroduced GFP-p62 as indicated to the right, were transfected with mCherry-EYFP-TRIM27. One day post transfection half of the cells were treated with HBSS for 2 hrs, before all cells were fixated, stained with DAPI and imaged using a Zeiss780 confocal microscope. Scale bar (10 μm). **D)** The graphs represent the amount of Yellow dots and RedOnly dots in the mCherry-EYFP-TRIM27 transfected cells shown with representative images in (**C**). The graphs are representing an average of 3 independent experiments. Normal (FM) and starved (HBSS 2hrs) (SM) conditions.

Figure 2: TRIM27 colocalizes- and interacts with ATG8s and SLRs, and has a LIR with specificity towards LC3C. A) Western blot analysis of endogenous TRIM27 in wild type HeLa cells and HeLa ATG7 KO cells (upper panel), or HeLa cells and HeLa penta KO cells (middle panel) or HeLa and HeLa ATG8 KO cells in normal medium (FM) or treated with HBSS (SM), Bafilomycin A1 (Baf) and MG132 (MG) for 4 hours. The numbers below the blot represent the intensity of the TRIM27 band correlated to PCNA quantitated using ImageJ, and is representative of two independent experiments. PCNA represent the loading control, while p62 and LC3B are controls of autophagy flux. * indicates an unspecific band. **B)** HEK293 FlpIn EGFP-TRIM27 cells were fixed and stained with antibodies for LC3B and p62. Images were obtained using a ZEISS780 confocal laser scanning microscope, and the co-localization monitored using the ZEN software**.** Scale bar (10 μm). **C)** Schematic representation of the domain architecture of TRIM27 with RING, B-box, Coiled-Coil (CC), LIR, and PRY/SPRY

domains indicated. Peptide array with 20-mers spanning the complete region of TRIM27 to define the peptides of TRIM27 able to interact with recombinant GST-GABARAP. The peptide walk was done with steps of three amino acid from one spot to the next. C, a two-dimensional peptide array scan analyzing the effects of single amino acid substitutions at all positions of the indicated 18-mer peptides from FYCO1 (amino acids 1276 –1293). The peptide arrays were probed with 1μg/ml GST-GABARAP for 2 h, and binding to GST-GABARAP was detected with anti-GST antibodies. The identified putative LIR is highlighted by stars and shadowed background in the amino acid sequence. **D)** GST-pulldown assay using ^{35}S-labeled Myc-TRIM27 or ^{35}S-labeled Myc-TRIM27$^{W184A/F186A/L189A}$ (LIRm) and recombinant GST and GST-ATG8 proteins. The amount of Myc-TRIM27 or Myc-TRIM27 LIRm bound to the various ATG8 proteins was detected by autoradiography. The numbers below represent the band intensities of bound TRIM27 as percentage of input band. The assay was repeated with similar results. **E)** The left panels show GST-pulldown assay using cell extracts from HEK293 FlpIn EGFP-TRIM27 cells and GST or GST-ATG8 proteins as indicated, immobilized on Glutathione Sepharose beads. EGFP-TRIM27 was detected using an anti-GFP antibody. GST proteins were visualized by Ponceau staining. The right panels show GST-pulldown assays using ^{35}S-labeled Myc-TRIM27 and recombinant GST, GST-p62 or GST-NDP52 immobilized on Glutathione Sepharose beads

Figure 3: TRIM27 KO impair selective autophagy response upon nucleotide induced stress. A) Representative images of HEK293 FlpIn and HEK293 FlpIn TRIM27 KO cells in full media (FM) or starved with HBSS (2 hrs) (SM) fixed and stained with antibodies for LC3B, p62, and WIPI2. Images were obtained using a ZEISS780 confocal laser scanning microscope, and the co-localization monitored using the ZEN software**.** Scale bar (10 μm), on inserts (2 μm). Arrows indicate colocalisation of LC3B, p62 and WIPI2. **B)** Western blot analysis of endogenous TRIM27, LC3B, TBK1 and Beclin1 in HEK293 FlpIn and HEK293 FlpIn TRIM27 KO cells. The cells were treated with the indicated substrates HBSS (SM) or BafA1 (200 nM) for 4 hours, before cell extracts were harvested in 1xSDS. 10 μg of the various cell extracts were separated on SDS-PAGE gels and blotted against the indicated antibodies. * indicates an unspecific band, an un-identified protein detected by the TRIM27 antibody. **C)** Western blot analysis of TRIM27 and p62 protein levels in HEK293 FlpIn, HEK293 FlpIn TRIM27 KO and HEK293 FlpIn EGFP-TRIM27 CD cells. The cells were treated with HBSS (SM) for 4 hours or transfected with a plasmid expressing the Myc tag only the day before harvesting (Myc), before cell extracts were harvested in 1xSDS. 10 μg of the various cell extracts were separated

on SDS-PAGE gels and blotted against the indicated antibodies. The bar graphs on top panel represent the average band intensities of p62/PCNA estimated by ImageJ from three independent experiments, with s.e.m. * indicates an unspecific band, an un-identified protein detected by the TRIM27 antibody. **D)** Western blot analysis of TRIM27 and LC3B protein levels in HEK293 FlpIn, HEK293 FlpIn TRIM27 KO and HEK293 FlpIn EGFP-TRIM27 CD cells. The cells were treated with HBSS (SM) for 4 hours or transfected with a plasmid expressing the Myc tag only the day before harvesting (Myc), before cell extracts were harvested in 1xSDS. 10 μg of the various cell extracts were separated on SDS-PAGE gels and blotted against the indicated antibodies. The bar graphs on top panel represent the average band intensities of unlipidated LC3B/PCNA estimated by ImageJ from three independent experiments, with s.e.m. **E)** Western blot analysis of TRIM27 and p62 protein levels in HEK293 FlpIn and HEK293 FlpIn TRIM27 KO cells. The cells were treated with the indicated substrates HBSS (SM)**,** poly (IC) or poly (AT) for 4 hours, before cell extracts were harvested in 1xSDS. 10 μg of the various cell extracts were separated on SDS-PAGE gels and blotted against the indicated antibodies. * indicates unspecific bands.

Figure 4: TRIM27 facilitates cell migration, is highly expressed in breast cancer tissues and inversely correlated with LC3B expression in various breast cancer cell lines. A) Western blot analysis of EGFP and EGFP-TRIM27 in cell extracts from HEK293 FlpIn TRIM27 KO cells reconstituted with EGFP or EGFP-TRIM27 (left panel). Expression was induced by Tetracycline (1 μg/ml) for 24 hrs as indicated. The right panels show confocal images of tetracycline-induced expression of EGFP-TRIM27 in the reconstituted HEK293 FlpIn TRIM27 KO cells under normal (FM) and starved (HBSS 2hrs) (SM) conditions. **B)** Proliferation (left graph) and migration (right graph) curves of HEK293 FlpIn, HEK293 FlpIn TRIM27 KO, and HEK293 FlpIn TRIM27 KO reconstituted with EGFP-TRIM27. The graphs were obtained using the IncuCyte® S3 Live-Cell Analysis System (Sartorius). Error bars indicate s.d. of independent experiments (n=3 for Proliferation, n=2 for migration). **C)** Graphs representing the TRIM27 mRNA (log2) expression levels in breast cancer tissues compared to normal tissues. The left graph represents average TRIM27 mRNA expression in breast cancer tissue compared to normal tissue in the same patients (n=23). The right graph represents average TRIM27 mRNA expression in tissue from healty individuals (n=5) compared to average TRIM27 mRNA expression in breast cancer tissue from patients (n=53). **D)** Western blot analysis of endogenous TRIM27 and LC3B in cell extracts from nine different breast cancer

cell lines representing different breast cancer subtypes. The blot is representative of three independent experiments.

REFERENCES

ALEMU, E. A., LAMARK, T., TORGERSEN, K. M., BIRGISDOTTIR, A. B., LARSEN, K. B., JAIN, A., OLSVIK, H., OVERVATN, A., KIRKIN, V. & JOHANSEN, T. 2012. ATG8 family proteins act as scaffolds for assembly of the ULK complex: sequence requirements for LC3-interacting region (LIR) motifs. *J Biol Chem,* 287**,** 39275-90.

BJORKOY, G., LAMARK, T., BRECH, A., OUTZEN, H., PERANDER, M., OVERVATN, A., STENMARK, H. & JOHANSEN, T. 2005. p62/SQSTM1 forms protein aggregates degraded by autophagy and has a protective effect on huntingtin-induced cell death. *J Cell Biol,* 171**,** 603-14.

CAI, J., CHEN, H. Y., PENG, S. J., MENG, J. L., WANG, Y., ZHOU, Y., QIAN, X. P., SUN, X. Y., PANG, X. W., ZHANG, Y. & ZHANG, J. 2018. USP7-TRIM27 axis negatively modulates antiviral type I IFN signaling. *FASEB J,* 32**,** 5238-5249.

CAO, T., DUPREZ, E., BORDEN, K. L., FREEMONT, P. S. & ETKIN, L. D. 1998. Ret finger protein is a normal component of PML nuclear bodies and interacts directly with PML. *J Cell Sci,* 111 (Pt 10)**,** 1319-29.

CAO, T., SHANNON, M., HANDEL, M. A. & ETKIN, L. D. 1996. Mouse ret finger protein (rfp) proto-oncogene is expressed at specific stages of mouse spermatogenesis. *Dev Genet,* 19**,** 309-20.

CHEN, L., HUANG, J., JI, Y., ZHANG, X., WANG, P., DENG, K., JIANG, X., MA, G. & LI, H. 2016. Tripartite motif 32 prevents pathological cardiac hypertrophy. *Clin Sci (Lond),* 130**,** 813-28.

COLELLA, B., FAIENZA, F. & DI BARTOLOMEO, S. 2019. EMT Regulation by Autophagy: A New Perspective in Glioblastoma Biology. *Cancers (Basel),* 11.

CONWELL, S. E., WHITE, A. E., HARPER, J. W. & KNIPE, D. M. 2015. Identification of TRIM27 as a novel degradation target of herpes simplex virus 1 ICP0. *J Virol,* 89**,** 220-9.

DIKIC, I. 2017. Proteasomal and Autophagic Degradation Systems. *Annu Rev Biochem,* 86**,** 193-224.

DOOLEY, H. C., RAZI, M., POLSON, H. E., GIRARDIN, S. E., WILSON, M. I. & TOOZE, S. A. 2014. WIPI2 links LC3 conjugation with PI3P, autophagosome formation, and pathogen clearance by recruiting Atg12-5-16L1. *Mol Cell,* 55**,** 238-52.

ESPOSITO, D., KOLIOPOULOS, M. G. & RITTINGER, K. 2017. Structural determinants of TRIM protein function. *Biochem Soc Trans,* 45**,** 183-191.

FORSHEY, B. M., SHI, J. & AIKEN, C. 2005. Structural requirements for recognition of the human immunodeficiency virus type 1 core during host restriction in owl monkey cells. *J Virol,* 79**,** 869-75.

HAMEED, O., PERRY, A., BANERJEE, R., ZHU, X. & PFEIFER, J. D. 2009. Papillary carcinoma of the breast lacks evidence of RET rearrangements despite morphological similarities to papillary thyroid carcinoma. *Mod Pathol,* 22**,** 1236-42.

HAO, Y. H., FOUNTAIN, M. D., JR., FON TACER, K., XIA, F., BI, W., KANG, S. H., PATEL, A., ROSENFELD, J. A., LE CAIGNEC, C., ISIDOR, B., KRANTZ, I. D., NOON, S. E., PFOTENHAUER, J. P., MORGAN, T. M., MORAN, R., PEDERSEN, R. C., SAENZ, M. S., SCHAAF, C. P. & POTTS, P. R. 2015. USP7 Acts as a Molecular Rheostat to Promote WASH-Dependent Endosomal Protein Recycling and Is Mutated in a Human Neurodevelopmental Disorder. *Mol Cell,* 59**,** 956-69.

HATAKEYAMA, S. 2017. TRIM Family Proteins: Roles in Autophagy, Immunity, and Carcinogenesis. *Trends Biochem Sci,* 42**,** 297-311.

HORIO, M., KATO, T., MII, S., ENOMOTO, A., ASAI, M., ASAI, N., MURAKUMO, Y., SHIBATA, K., KIKKAWA, F. & TAKAHASHI, M. 2012. Expression of RET finger protein predicts chemoresistance in epithelial ovarian cancer. *Cancer Med,* 1**,** 218-29.

IWAKOSHI, A., MURAKUMO, Y., KATO, T., KITAMURA, A., MII, S., SAITO, S., YATABE, Y. & TAKAHASHI, M. 2012. RET finger protein expression is associated with prognosis in lung cancer with epidermal growth factor receptor mutations. *Pathol Int,* 62**,** 324-30.

JI, C. H. & KWON, Y. T. 2017. Crosstalk and Interplay between the Ubiquitin-Proteasome System and Autophagy. *Mol Cells,* 40**,** 441-449.

KARANASIOS, E., STAPLETON, E., MANIFAVA, M., KAIZUKA, T., MIZUSHIMA, N., WALKER, S. A. & KTISTAKIS, N. T. 2013. Dynamic association of the ULK1 complex with omegasomes during autophagy induction. *J Cell Sci,* 126**,** 5224-38.

KEOWN, J. R., BLACK, M. M., FERRON, A., YAP, M., BARNETT, M. J., PEARCE, F. G., STOYE, J. P. & GOLDSTONE, D. C. 2018. A helical LC3-interacting region mediates the interaction between the retroviral restriction factor Trim5alpha and mammalian autophagy-related ATG8 proteins. *J Biol Chem,* 293**,** 18378-18386.

KIMURA, T., JAIN, A., CHOI, S. W., MANDELL, M. A., SCHRODER, K., JOHANSEN, T. & DERETIC, V. 2015. TRIM-mediated precision autophagy targets cytoplasmic regulators of innate immunity. *J Cell Biol,* 210**,** 973-89.

KIMURA, T., MANDELL, M. & DERETIC, V. 2016. Precision autophagy directed by receptor regulators - emerging examples within the TRIM family. *J Cell Sci,* 129**,** 881-91.

KLEIGER, G. & MAYOR, T. 2014. Perilous journey: a tour of the ubiquitin-proteasome system. *Trends Cell Biol,* 24**,** 352-9.

KOYAMA-HONDA, I., ITAKURA, E., FUJIWARA, T. K. & MIZUSHIMA, N. 2013. Temporal analysis of recruitment of mammalian ATG proteins to the autophagosome formation site. *Autophagy,* 9**,** 1491-9.

KUO, C. J., HANSEN, M. & TROEMEL, E. 2018. Autophagy and innate immunity: Insights from invertebrate model organisms. *Autophagy,* 14**,** 233-242.

KWON, Y. T. & CIECHANOVER, A. 2017. The Ubiquitin Code in the Ubiquitin-Proteasome System and Autophagy. *Trends Biochem Sci*.

LAMARK, T., PERANDER, M., OUTZEN, H., KRISTIANSEN, K., OVERVATN, A., MICHAELSEN, E., BJORKOY, G. & JOHANSEN, T. 2003. Interaction codes within the family of mammalian Phox and Bem1p domain-containing proteins. *J Biol Chem,* 278**,** 34568-81.

LIU, Y., ZHU, M., LIN, L., FAN, X., PIAO, Z. & JIANG, X. 2014. Deficiency of Trim27 protects dopaminergic neurons from apoptosis in the neurotoxin model of Parkinson's disease. *Brain Res,* 1588**,** 17-24.

MA, Y., WEI, Z., BAST, R. C., JR., WANG, Z., LI, Y., GAO, M., LIU, Y., WANG, X., GUO, C., ZHANG, L. & WANG, X. 2016. Downregulation of TRIM27 expression inhibits the proliferation of ovarian cancer cells in vitro and in vivo. *Lab Invest,* 96**,** 37-48.

MANDELL, M. A., JAIN, A., ARKO-MENSAH, J., CHAUHAN, S., KIMURA, T., DINKINS, C., SILVESTRI, G., MUNCH, J., KIRCHHOFF, F., SIMONSEN, A., WEI, Y., LEVINE, B., JOHANSEN, T. & DERETIC, V. 2014a. TRIM proteins regulate autophagy and can target autophagic substrates by direct recognition. *Dev Cell,* 30**,** 394-409.

MANDELL, M. A., JAIN, A., KUMAR, S., CASTLEMAN, M. J., ANWAR, T., ESKELINEN, E. L., JOHANSEN, T., PREKERIS, R. & DERETIC, V. 2016. TRIM17 contributes to autophagy of midbodies while actively sparing other targets from degradation. *J Cell Sci,* 129**,** 3562-3573.

MANDELL, M. A., KIMURA, T., JAIN, A., JOHANSEN, T. & DERETIC, V. 2014b. TRIM proteins regulate autophagy: TRIM5 is a selective autophagy receptor mediating HIV-1 restriction. *Autophagy,* 10**,** 2387-8.

OVERÅ, K., GARCIA, J.G., BHUJABAL, Z., JAIN, A., ØVERVATN, A., LARSEN, K.B., DERETIC, V., JOHANSEN, T., LAMARK, T., AND SJØTTEM, E. 2019. TRIM32, but not its muscular dystrophy-associated mutant, positively regulates and is targeted to autophagic degradation by p62/SQSTM. *J. Cell Science.* PMID 31828304.

PANKIV, S., CLAUSEN, T. H., LAMARK, T., BRECH, A., BRUUN, J. A., OUTZEN, H., OVERVATN, A., BJORKOY, G. & JOHANSEN, T. 2007. p62/SQSTM1 binds directly to Atg8/LC3 to facilitate degradation of ubiquitinated protein aggregates by autophagy. *J Biol Chem,* 282**,** 24131-45.

POLSON, H. E., DE LARTIGUE, J., RIGDEN, D. J., REEDIJK, M., URBE, S., CLAGUE, M. J. & TOOZE, S. A. 2010. Mammalian Atg18 (WIPI2) localizes to omegasome-anchored phagophores and positively regulates LC3 lipidation. *Autophagy,* 6**,** 506-22.

RAN, F. A., HSU, P. D., WRIGHT, J., AGARWALA, V., SCOTT, D. A. & ZHANG, F. 2013. Genome engineering using the CRISPR-Cas9 system. *Nat Protoc,* 8**,** 2281-2308.

SWATEK, K. N. & KOMANDER, D. 2016. Ubiquitin modifications. *Cell Res,* 26**,** 399-422.

TAKAHASHI, M. & COOPER, G. M. 1987. ret transforming gene encodes a fusion protein homologous to tyrosine kinases. *Mol Cell Biol,* 7**,** 1378-85.

TEZEL, G., NAGASAKA, T., IWAHASHI, N., ASAI, N., IWASHITA, T., SAKATA, K. & TAKAHASHI, M. 1999. Different nuclear/cytoplasmic distributions of RET finger protein in different cell types. *Pathol Int,* 49**,** 881-6.

TEZEL, G. G., UNER, A., YILDIZ, I., GULER, G. & TAKAHASHI, M. 2009. RET finger protein expression in invasive breast carcinoma: relationship between RFP and ErbB2 expression. *Pathol Res Pract,* 205**,** 403-8.

TOMAR, D., SINGH, R., SINGH, A. K., PANDYA, C. D. & SINGH, R. 2012. TRIM13 regulates ER stress induced autophagy and clonogenic ability of the cells. *Biochim Biophys Acta,* 1823**,** 316-26.

TOWNSON, S. M., KANG, K., LEE, A. V. & OESTERREICH, S. 2006. Novel role of the RET finger protein in estrogen receptor-mediated transcription in MCF-7 cells. *Biochem Biophys Res Commun,* 349**,** 540-8.

TSUKAMOTO, H., KATO, T., ENOMOTO, A., NAKAMURA, N., SHIMONO, Y., JIJIWA, M., ASAI, N., MURAKUMO, Y., SHIBATA, K., KIKKAWA, F. & TAKAHASHI, M. 2009. Expression of Ret finger protein correlates with outcomes in endometrial cancer. *Cancer Sci,* 100**,** 1895-901.

VON MUHLINEN, N., AKUTSU, M., RAVENHILL, B. J., FOEGLEIN, A., BLOOR, S., RUTHERFORD, T. J., FREUND, S. M., KOMANDER, D. & RANDOW, F. 2012. LC3C, bound selectively by a noncanonical LIR motif in NDP52, is required for antibacterial autophagy. *Mol Cell,* 48**,** 329-42.

WANG, J., TENG, J. L., ZHAO, D., GE, P., LI, B., WOO, P. C. & LIU, C. H. 2016. The ubiquitin ligase TRIM27 functions as a host restriction factor antagonized by Mycobacterium tuberculosis PtpA during mycobacterial infection. *Sci Rep,* 6**,** 34827.

YU, H. & MATOUSCHEK, A. 2017. Recognition of Client Proteins by the Proteasome. *Annu Rev Biophys,* 46**,** 149-173.

ZHANG, H. X., XU, Z. S., LIN, H., LI, M., XIA, T., CUI, K., WANG, S. Y., LI, Y., SHU, H. B. & WANG, Y. Y. 2018a. TRIM27 mediates STAT3 activation at retromer-positive structures to promote colitis and colitis-associated carcinogenesis. *Nat Commun,* 9**,** 3441.

ZHANG, Y., FENG, Y., JI, D., WANG, Q., QIAN, W., WANG, S., ZHANG, Z., JI, B., ZHANG, C., SUN, Y. & FU, Z. 2018b. TRIM27 functions as an oncogene by activating epithelial-mesenchymal transition and p-AKT in colorectal cancer. *Int J Oncol,* 53**,** 620-632.

ZHENG, Q., HOU, J., ZHOU, Y., YANG, Y., XIE, B. & CAO, X. 2015. Siglec1 suppresses antiviral innate immune response by inducing TBK1 degradation via the ubiquitin ligase TRIM27. *Cell Res,* 25**,** 1121-36.

ZHUANG, X. J., TANG, W. H., FENG, X., LIU, C. Y., ZHU, J. L., YAN, J., LIU, D. F., LIU, P. & QIAO, J. 2016. Trim27 interacts with Slx2, is associated with meiotic processes during spermatogenesis. *Cell Cycle,* 15**,** 2576-2584.

ZOUMPOULIDOU, G., BROCENO, C., LI, H., BIRD, D., THOMAS, G. & MITTNACHT, S. 2012. Role of the tripartite motif protein 27 in cancer development. *J Natl Cancer Inst,* 104**,** 941-52.

ZUREK, B., SCHOULTZ, I., NEERINCX, A., NAPOLITANO, L. M., BIRKNER, K., BENNEK, E., SELLGE, G., LERM, M., MERONI, G., SODERHOLM, J. D. & KUFER, T. A. 2012. TRIM27 negatively regulates NOD2 by ubiquitination and proteasomal degradation. *PLoS One,* 7**,** e41255.

Figure 1

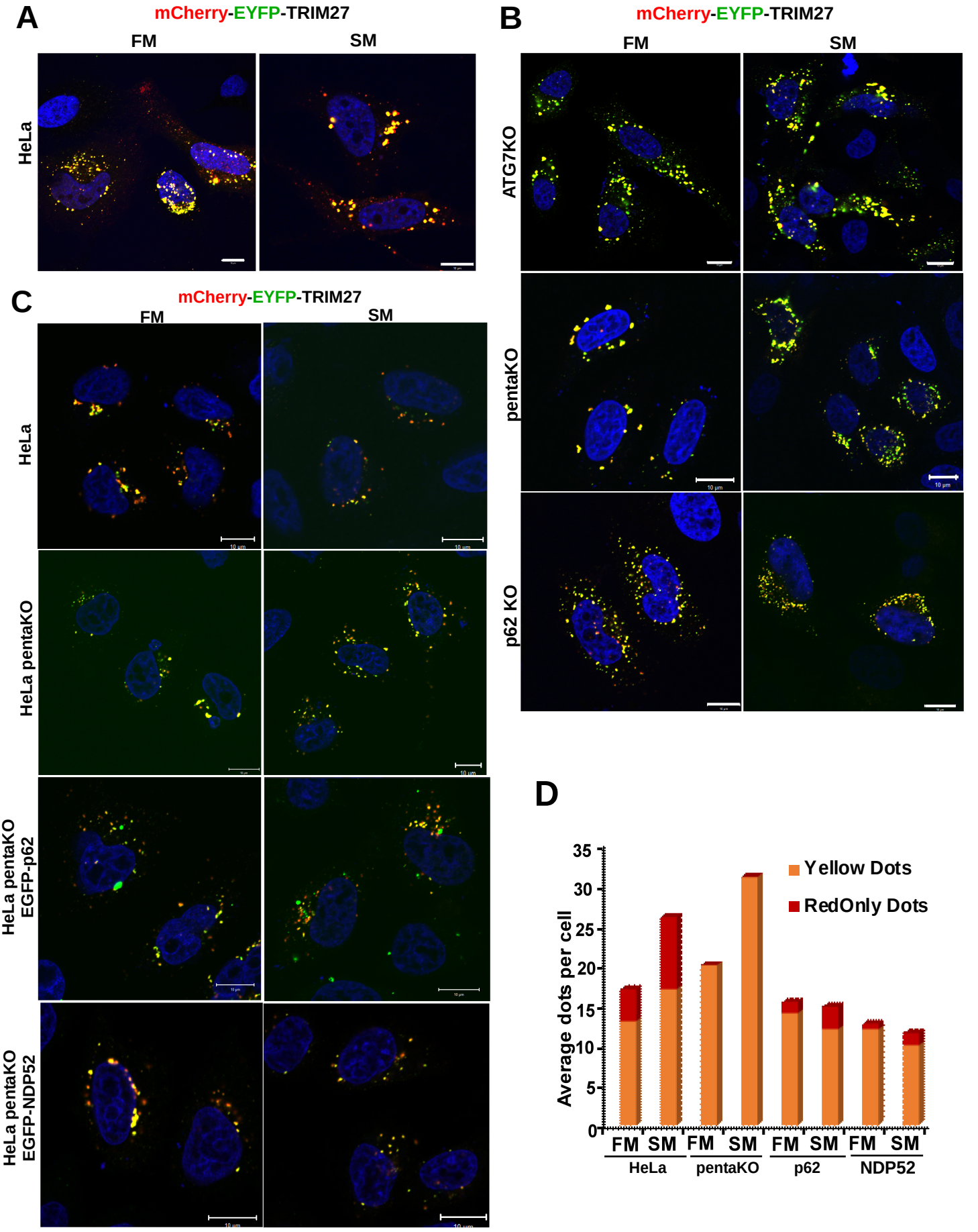
A
mCherry-EYFP-TRIM27
FM
SM
HeLa
B
mCherry-EYFP-TRIM27
FM
SM
ATG7KO
pentaKO
p62 KO
C
mCherry-EYFP-TRIM27
FM
SM
HeLa
HeLa pentaKO
HeLa pentaKO EGFP-p62
HeLa pentaKO EGFP-NDP52
D
Average dots per cell
0
5
10
15
20
25
30
35
Yellow Dots
RedOnly Dots
FM SM FM SM FM SM FM SM
HeLa
pentaKO
p62
NDP52

Figure 2

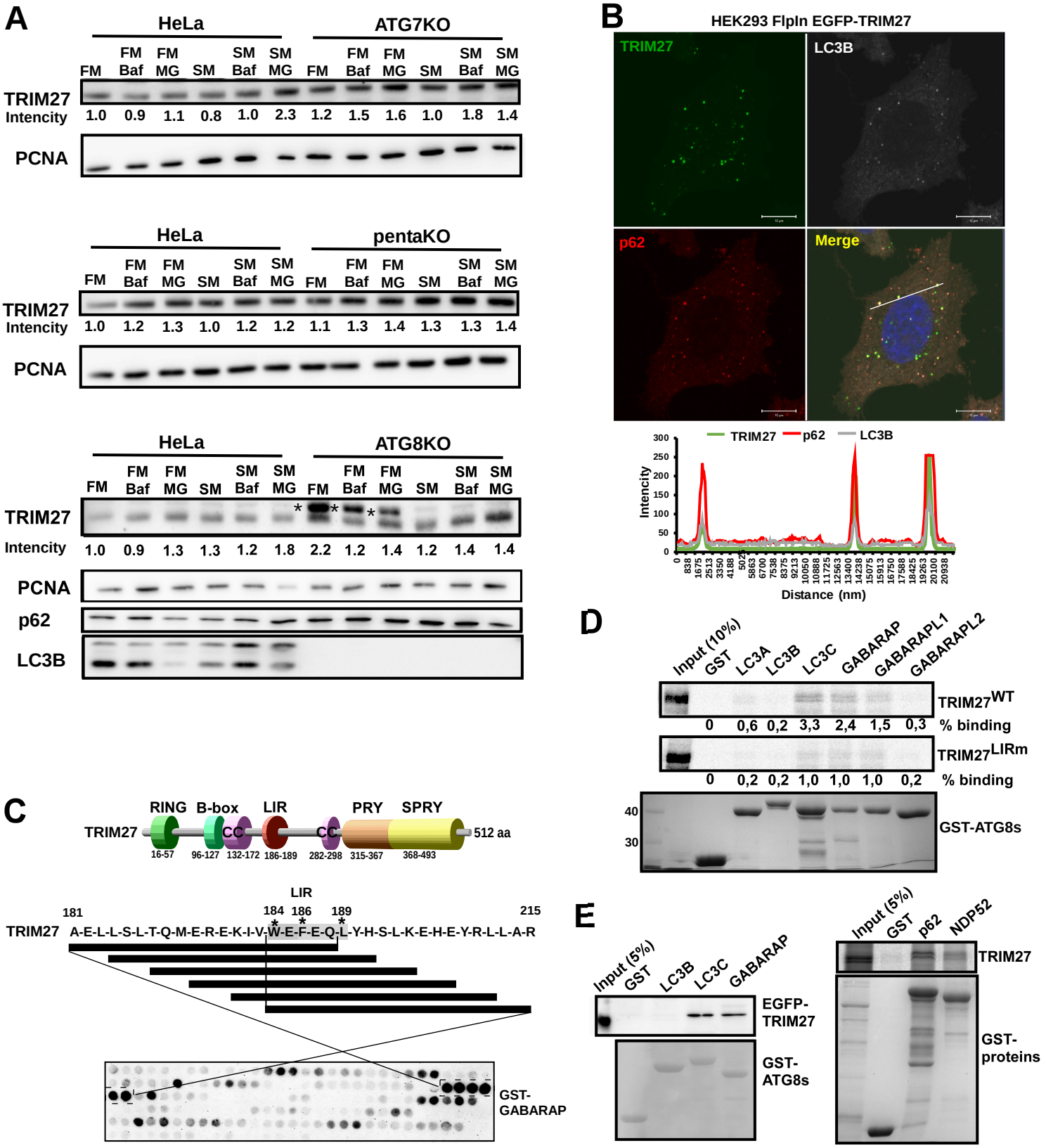
A
HeLa
ATG7KO
FM
FM Baf
FM MG
SM
SM Baf
SM MG
TRIM27
Intencity
1.0 0.9 1.1 0.8 1.0 2.3 1.2 1.5 1.6 1.0 1.8 1.4
PCNA
HeLa
pentaKO
1.0 1.2 1.3 1.0 1.2 1.2 1.1 1.3 1.4 1.3 1.3 1.4
HeLa
ATG8KO
1.0 0.9 1.3 1.3 1.2 1.8 2.2 1.2 1.4 1.2 1.4 1.4
p62
LC3B
B
HEK293 FlpIn EGFP-TRIM27
TRIM27
LC3B
p62
Merge
TRIM27 p62 LC3B
Intensity
Distance (nm)
C
TRIM27
RING B-box CC LIR CC PRY SPRY
512 aa
16-57 96-127 132-172 186-189 282-298 315-367 368-493
LIR
181 184 186 189 215
A-E-L-L-S-L-T-Q-M-E-R-E-K-I-V-W-E-F-E-Q-L-Y-H-S-L-K-E-H-E-Y-R-L-L-A-R
GST-GABARAP
D
Input (10%)
GST
LC3A
LC3B
LC3C
GABARAP
GABARAPL1
GABARAPL2
TRIM27WT
0 0,6 0,2 3,3 2,4 1,5 0,3
% binding
TRIM27LIRm
0 0,2 0,2 1,0 1,0 1,0 0,2
% binding
40
30
GST-ATG8s
E
Input (5%)
GST
LC3B
LC3C
GABARAP
EGFP-TRIM27
GST-ATG8s
Input (5%)
GST
p62
NDP52
TRIM27
GST-proteins

Figure 3

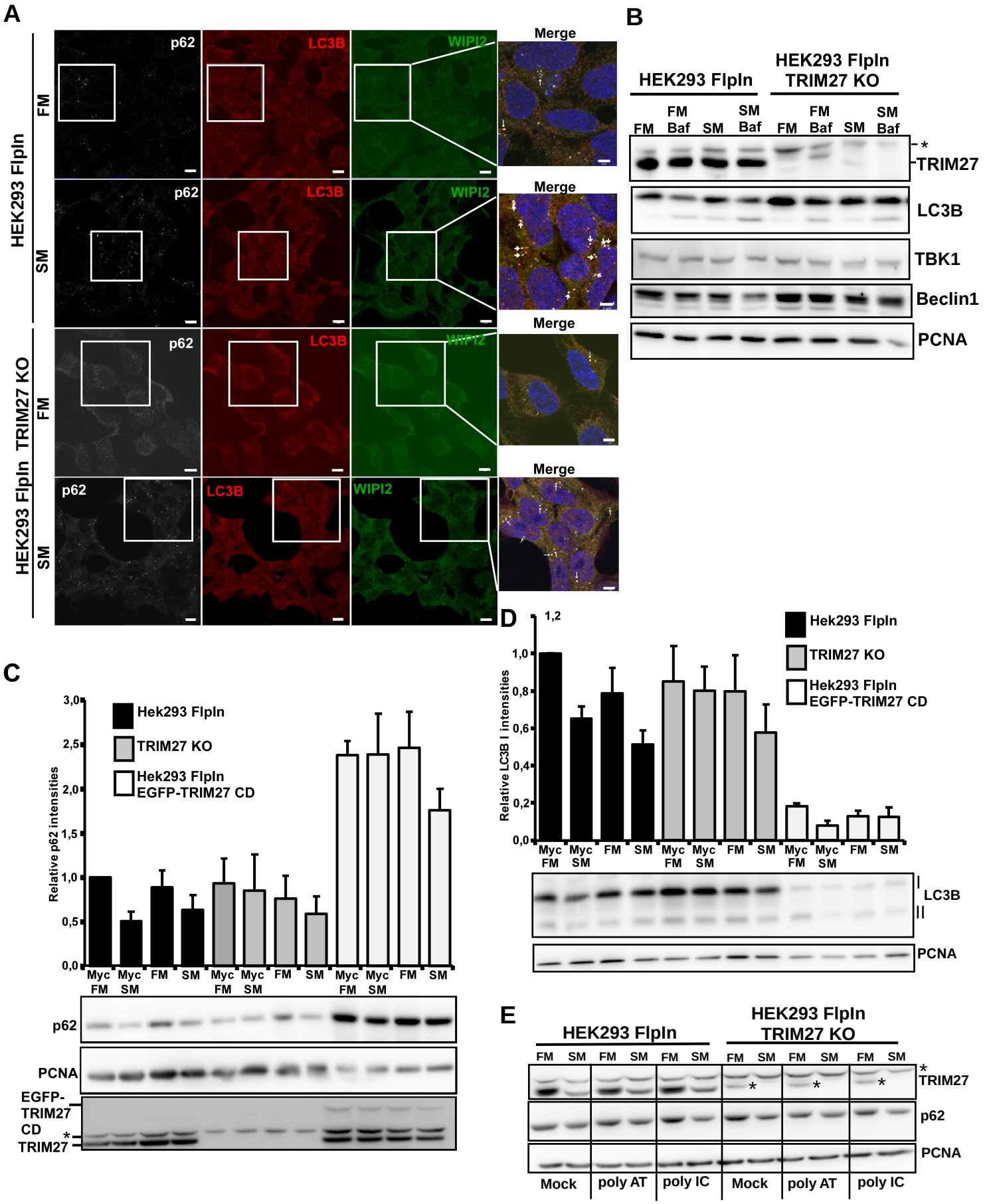
A
HEK293 FlpIn
TRIM27 KO
FM
SM
p62
LC3B
WIPI2
Merge
B
HEK293 FlpIn
HEK293 FlpIn TRIM27 KO
FM
FM Baf
SM
SM Baf
TRIM27
LC3B
TBK1
Beclin1
PCNA
C
Hek293 FlpIn
TRIM27 KO
Hek293 FlpIn EGFP-TRIM27 CD
Relative p62 intensities
Myc FM
Myc SM
p62
PCNA
EGFP-TRIM27 CD
TRIM27
D
Relative LC3B I intensities
LC3B
PCNA
E
HEK293 FlpIn
HEK293 FlpIn TRIM27 KO
TRIM27
p62
PCNA
Mock
poly AT
poly IC

Figure 4

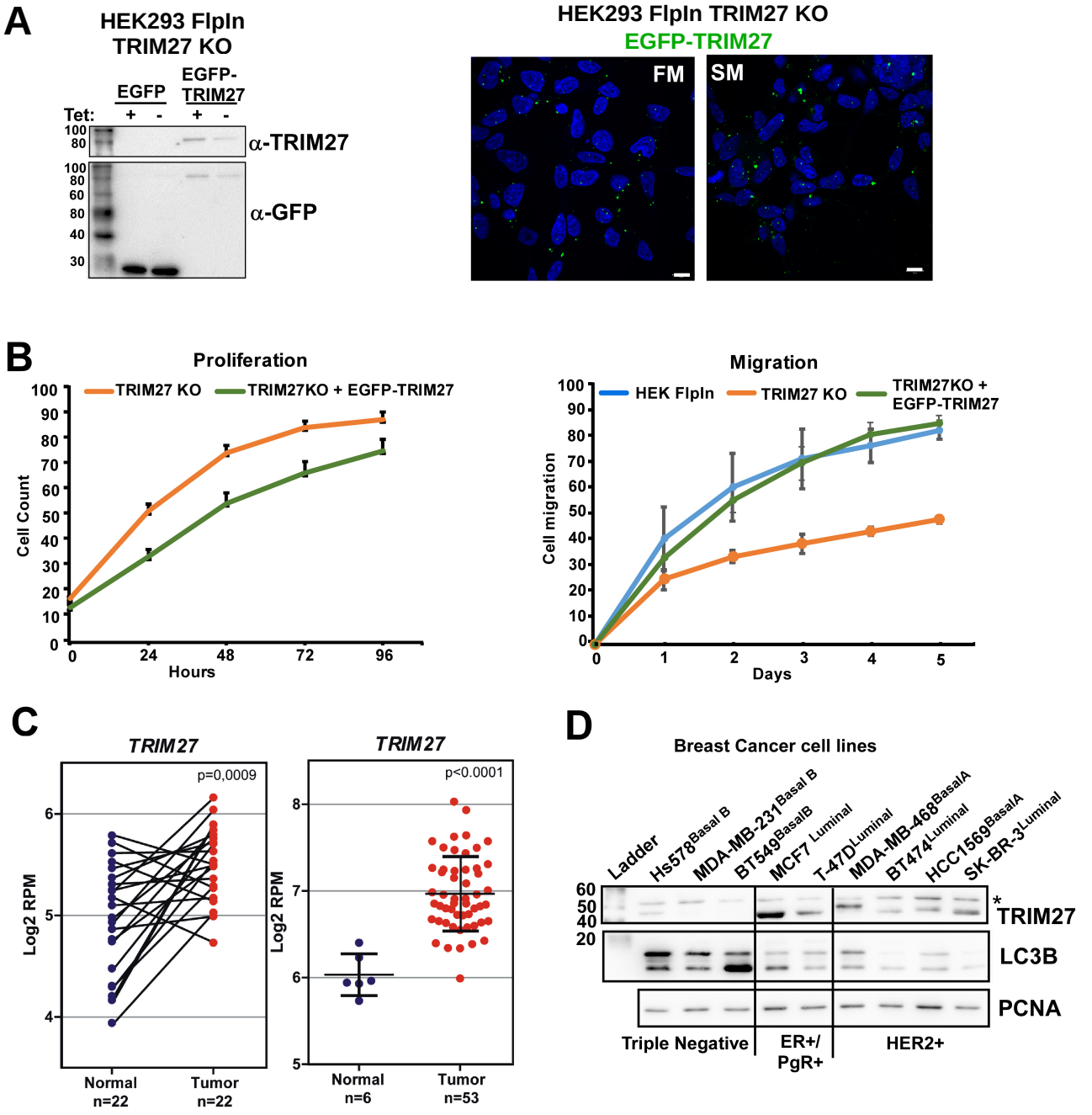
A
HEK293 FlpIn TRIM27 KO
EGFP
EGFP-TRIM27
Tet: + - + -
100
80
α-TRIM27
100
80
60
80
40
30
α-GFP
HEK293 FlpIn TRIM27 KO
EGFP-TRIM27
FM
SM
B
Proliferation
TRIM27 KO
TRIM27KO + EGFP-TRIM27
Cell Count
Hours
0
24
48
72
96
Migration
HEK FlpIn
TRIM27 KO
TRIM27KO + EGFP-TRIM27
Cell migration
Days
0
1
2
3
4
5
C
TRIM27
p=0,0009
Log2 RPM
Normal n=22
Tumor n=22
TRIM27
p<0.0001
Log2 RPM
Normal n=6
Tumor n=53
D
Breast Cancer cell lines
Ladder
Hs578Basal B
MDA-MB-231Basal B
BT549BasalB
MCF7 Luminal
T-47DLuminal
MDA-MB-468BasalA
BT474Luminal
HCC1569BasalA
SK-BR-3Luminal
60
50
40
20
*TRIM27
LC3B
PCNA
Triple Negative
ER+/ PgR+
HER2+